Nanoscale crystallinity modulates cell proliferation on plasma sprayed surfaces

Journal Item

Nanoscale crystallinity modulates cell proliferation on plasma sprayed surfaces

Alan M Smith[2], Jennifer Z Paxton[1], Yi-Pei Hung[1], Martin J Hadley[1], James Bowen[1], Richard L Williams and Liam M Grover[1 *]

[1]School of Chemical Engineering, University of Birmingham, Edgbaston, B15 2TT, UK

[2]School of Applied Sciences, University of Huddersfield, Huddersfield, HD1 3DH, UK

*author to whom all correspondence should be addressed

Email: l.m.grover@bham.ac.uk

Tel: +44 121 414 3887

Fax: +44 121 414 5324

Keywords: prosthesis; calcium phosphate; hydroxyapatite; coating; crystallinity

Abstract

Calcium phosphate coatings have been applied to the surface of metallic prostheses to mediate hard and soft tissue attachment for more than 40 years. Most coatings are formed of high purity hydroxyapatite, and coating methods are often designed to produce highly crystalline surfaces. It is likely however, that coatings of lower crystallinity can facilitate more rapid tissue attachment since the surface will exhibit a higher specific surface area and will be considerably more reactive than a comparable highly crystalline surface. Here we test this hypothesis by growing a population of MC3T3 osteoblast-like cells on the surface of two types of hip prosthesis with similar composition, but with differing crystallinity. The surfaces with lower crystallinity facilitated more rapid cell attachment and increased proliferation rate, despite having a less heterogeneous surface topography. This work highlights that the influence of the crystallinity of HA at the nano-scale is dominant over macro-scale topography for cell adhesion and growth. Furthermore, crystallinity could be easily adjusted by without compromising coating purity. These findings could facilitate designing novel coated calcium phosphate surfaces that more rapidly bond tissue following implantation.

1. Introduction

Hydroxyapatite (HA) is the main mineral constituent of bone comprising almost 70 wt% of the mass of our skeleton. Since HA is relatively simple to synthesise using both wet chemical and reactive sintering routes, it has been widely investigated for use as a bone graft replacement [1, 2, 3]. The osteoconductive nature of the HA also means that it has found significant use as coating on metallic implants, where it can facilitate the attachment of both hard and soft tissues and allow firm attachment of the prosthesis *in vivo* [4].

There are a multitude of methods that have been employed to coat metallic prostheses with HA, which have recently been reviewed in detail [5]. The majority of clinically available prostheses, however, are coated using a high temperature plasma in which the HA is 'melted' before deposition on the implant surface [6]. It is possible to adjust the composition and crystallinity of the deposited coating however, by varying gas phase, atmospheric pressure and anode current. The use of high energy coating conditions can result in a considerable reduction in crystallinity [7], which may be coupled with the deposition of impurity phases within the coating. These impurities may include tetracalcium phosphate ($Ca_4(PO_4)_3O$), calcium oxide (CaO), amorphous calcium phosphate (ACP; $Ca_xH_y(PO_4)_z.nH_2O$), β-tricalcium phosphate (β-TCP; $Ca_3(PO_4)_2$) and oxyapatite ($Ca_{10}(PO_4)_6O$) [8, 9]. The formation of these phases within the implant coating has been shown to result in the accelerated localised dissolution of the coating [10]. Numerous workers have striven to eradicate the formation of these impurity phases from the coating [8, 9, 10]. As a consequence, the majority of commercially available calcium phosphate coatings are formed from highly crystalline HA. Although easy to characterise using X-ray diffraction and required by some standards, one might expect that the high crystallinity and low solubility of the HA deposited on the majority of prostheses would result in suboptimal early-stage tissue

attachment. Other materials which facilitate bone attachment, such as bioglass, are thought to form an intimate adhesion with bone through the dissolution of their surface and their subsequent re-precipitation in surrounding tissues [11]. While undoubtedly the localised dissolution of highly basic phases such as TTCP and CaO could have a deleterious biological reaction and so their formation should be avoided, it would seem surprising that more products are not based around the other more soluble calcium salts (ACP, oxyapatite etc.) that may facilitate this process.

In this study, the attachment of MC3T3 cells to the surface of two compositionally identical commercially available hydroxyapatite coated prostheses of distinct crystallinity has been investigated. The topography of both coatings was characterised using scanning electron microscopy and white light interferometry. Quantification of the crystallinity of the coatings was performed using X-ray diffraction and crystallite size was estimated from the XRD data using the Scherrer equation, while coating crystallinity was further varied by adjusting the anodic current during the coating process. In addition, elemental composition of the coatings was investigated using X-ray Fluorescence spectroscopy (XRF).

2. Materials and Methods

2.1 Preparation of prostheses

Two types of carbonated hydroxyapatite coated hip prosthesis with similar composition but contrasting crystallinities were sourced directly from manufacturers (JRI; Depuy). Both types of prosthesis were sectioned using a diamond saw in order to produce samples of appropriate geometry for seeding in standard 12 well plates. Prior to characterisation, the prostheses were

autoclaved for sterilisation. From here on, the prostheses will be referred to as group A (lower crystallinity) and group B (higher crystallinity).

2.2 Cell culture and attachment to prostheses

To evaluate cell attachment to each prosthesis coating, MC3T3 cells (European collection of cell cultures - ECACC) were defrosted and seeded into T150 flasks with Dulbecco's minimum essential medium (D-MEM) containing 10w/v% foetal bovine serum. After they reached confluency (approximately two days), the cells were removed from the surface of the culture flask using trypsin-EDTA, were redispersed in medium at a cell density of 4.05×10^5 cells per mL and were then passaged 3 times prior to surface seeding. Sterilised (by autoclave and UV radiation) surfaces were seeded with MC3T3 cells at a density of 1×10^5 cells per sample. The number of cells on the surface of the implants were counted on days 1, 9, and 21 and compared with the control (tissue culture plastic). For counting, the live cells were stained using Calcein (a fluorescent green stain which only stains live cells) and were then visualised using a fluorescence microscope. At least five areas of the surface were imaged and then fluorescent cells counted within the field (1 mm^2), and the average cell number per unit area of the surface was subsequently calculated. The data were collected for at least three samples in each sample set, making each result the average of 45 measurements.

2.3 SEM images

The surface morphologies of the coatings were evaluated using scanning electron microscopy. The unembedded prostheses were mounted on aluminium stubs using carbon tape. The surface of the prosthesis was subsequently sputtered with platinum to prevent the sample charging.

Following preparation, images were captured using a scanning electron microscope at an accelerating voltage of 10 kV. The embedded samples were examined using a scanning electron microscope forming an image using back scattered electrons, these images were used to determine the thickness of the implant coatings. The samples were unsputtered and charging was prevented by painting the sample surfaces using silver dag adhesive paint.

2.4 Interferometry

In order to enable quantitative characterisation of the topography of the calcium phosphate coatings, interferometric measurements of samples were performed using a MicroXAM interferometer (Scantron, UK), operating using a white light source. Samples were imaged at 31X magnification, acquiring images in a grid array which were subsequently stitched together. The final image had dimensions of 3.64mm x 2.71mm. Scanning Probe Image Processor software (Image Metrology, Denmark) was employed for the analysis of acquired images, yielding S_a and S_q values for surface roughness.

2.5 X-ray diffraction analysis

To characterise the crystalline component of the coating, the coating was carefully removed from the surface of the implant using a razor blade and X-Ray Diffraction measurements were carried out on the resulting powder using a Bruker D8 diffractometer, arranged in transmission mode using Cu Kα1 radiation (λ = 1.5406Å) between 5^o and 80^o 2-θ, with a step size of 0.0197^o and a step time of 0.2secs. The collected patterns were compared with JCPDS patterns for HA and any impurity phases likely to be found within the coating. The crystallinity of the coatings were compared by determining the area under the diffraction pattern for a strong peak indicative of the presence of HA. The resulting crystallinity of the material was normalised, so that the raw

powder was given a value of 100. It should be noted that this gives a relative and not absolute measurement of crystallinity. To evaluate the influence of process conditions on crystallinity, the coatings were deposited using vacuum plasma spraying and the anodic current was varied between 400-700 A. Crystallite size was estimated from the XRD data using the Scherrer equation:

$$X_s = \frac{0.9\lambda}{FWHM \cos\theta}$$

eqn. 1

where λ is the wavelength of the monochromatic X-ray beam (λ = 0.15406nm for CuKα radiation), FWHM is the full width at half maximum of the diffraction peak under analysis [radians] and θ is the Bragg angle at which the peak is located. Diffraction peaks at 2θ = 25.784° {002} and 2θ = 32.981° {300}, which correspond to the c- and a- axes of the HA crystal lattice, respectively. These peaks were chosen due their isolation from the other diffraction peaks (enabling a more reliable estimation of crystallite size) and as they represent the major axes of HA crystal growth. Fraction of crystalline phase, X_c, was estimated using the following equation:

$$X_c = 1 - \frac{V_{112/300}}{I_{300}}$$

eqn. 2

where $V_{112/300}$ is the intensity minimum between the {112} and {300} diffraction peaks of HA, and I_{300} is the intensity of the {300} diffraction peak of HA.

2.6 X-ray Fluorescence analysis

To identify the elemental composition of the coatings X-ray Fluorescence spectroscopy (XRF) was carried out using a S8 TIGER XRF spectrometer (Bruker Corp., U.S.A). Samples were prepared as described for the X-Ray Diffraction measurements.

2.7 Statistical analysis

The data were expressed as the mean ± the standard deviation and analysed using Primer for biostatistics software. For the analysis of the cell attachment data one way analysis of variance (ANOVA) was used with a post hoc Tukey (HSD) test to identify significant differences at a confidence limit of $P < 0.01$.

3. Results

3.1 Cell culture and attachment to prostheses

When seeded onto the surface of the prostheses, cell attachment was noted within one day of seeding on each of the surfaces investigated (Figure 1). The cells exhibited morphology typical of osteoblasts with an approximate diameter of 20 µm. At day one, the cells attached to the surface of Group A exhibited a polygonal morphology and those attached to the surface of the tissue culture plastic (Control) and Group B demonstrated a more spindle-like structure. As culture time increased, the morphologies of the cells on each surface exhibited a more polygonal morphology. Another major difference between the two test samples was the larger number of cells attached to Group A following day 1 of the study (Figure 1). When the number of cells on the prostheses and tissue culture plastic were quantified, the number of cells found per mm^2 of the material was significantly higher ($p<0.01$) for Group A (420 ± 135 cells) than for Group B (120 ± 10 cells) or the tissue culture plastic (175 ± 80 cells) (Figure 1). By 9 days of culture,

there was no significant difference between the number of cells on the surfaces and beyond this time-point, in the case of all groups there was a steady reduction in the number of cells found on the surface of the samples. After 21 days of attachment, regions of Group A seemed devoid of cells, suggesting that the cell culture had reached confluence resulting in cell death which was not apparent in Group B (Figure 1).

3.2 Prostheses topography

Since the attachment of cells to implant surface can be influenced by topographical variation, the topography of the coated samples was determined by means of scanning electron microscopy (SEM) and white light interferometry. At the highest level of magnification, each coating exhibited a similar structure with the presence of submicrometer irregularly shaped particles (Figure 2), although some more plate-like crystals were observable within the Group B coating. At lower levels of magnification, the coating on the surface of Group B seems marginally more pitted and irregular than the Group A coating, however, this is difficult to quantify using only scanning electron microscopy. Further characterisation of the surface coating was therefore undertaken using interferometry. From visual inspection of the surface profiles generated using the laser profilometer, the Group B coating appeared to be most irregular, although this is hard to quantify simply by inspection of Figure 3a. Quantitative analysis of the surface profiles demonstrated that there was virtually no differences between the surface area roughness (S_a) values for the samples (Figure 3b), with the Group A coating exhibiting an Sa of 11.94 ± 0.83 µm and the Group B coating an S_a of 11.78 ± 6.2 µm. The large standard deviation of the group B coating however is indicative of a more heterogeneous surface topography. This would theoretically favour more rapid attachment which was not the case in this study.

Since the contrast in early stage cell attachment cannot be explained by surface topography, the coated surfaces were further characterised with respect to their compositions, since composition is also known to have a significant influence on cell attachment.

3.3 X-ray diffraction and X-ray Fluorescence

The crystalline compositions of the calcium phosphate coatings were determined using X-ray diffraction. Both Groups A and B resulted in the formation of diffraction patterns that displayed the main peaks for hydroxyapatite, both with the presence of no crystalline impurity phases (Figure 4). Although the principle peaks for each of the coatings occurred in similar positions on the diffraction patterns, the morphology of the peaks collected from Group A and Group B contrasted significantly. The diffraction pattern collected from Group A contained significantly broader and less intense peaks than those found on the diffraction pattern for samples from Group B. The broader and less intense peaks both suggest that the calcium phosphate coating that was found on the surface of Group A was of lower crystallinity than that found on the Group B. This was verified by estimating the crystalline fraction of the coatings along with the crystallite size (Table 1), which showed that the crystals of Group A were smaller in both the c- and a-axes compared to Group B (in fact the {002} peak of Group A was too weak to permit a reliable estimation of crystallite size along this plane. In addition to reduced crystallite size, Group A was also found to have a lower crystalline fraction compared to Group B. As the crystallinity of the two coatings was the only significant difference between the coatings that could explain enhanced cell attachment of Group A, efforts were made to further reduce coating crystallinity by changing process parameters. Samples were therefore formed using the feedstock used for Group A but with anodic coating currents of 400, 500, 600 and 700 A. The resulting coatings were characterised using X-ray diffraction (Figure 5) and it was found that the

increased anodic potential resulted in a monotonic reduction in crystallinity (Figure 6). Importantly, although crystallinity was reduced by up to 60% (when compared with the raw powder) there was no detectable presence of impurity phases within the coated surface. This was further supported by the elemental analysis performed using XRF which detected Ca, P, low levels of Mg (which is typical in calcium phosphate coatings) and Ti (from underlying metallic surface) (Table 2).

4. Discussion

Despite previous efforts to produce HA coatings of extremely high purity and crystallinity [8, 9, 10,], there has recently been a realisation that the production of coatings which are comparable with the nanocrystalline HA found in the body could have significant benefits [12]. The higher specific surface area of nanocrystalline HA compared with microcrystalline HA means that the attachment of cell adhesive proteins and the localised dissolution of coating can be significantly increased [13, 14]. Consequently, a number of workers have sought to develop methods whereby metallic surfaces may be coated with HA based coatings without the need for heating, which can result in significant crystal growth. For example, authors have reported the production of coatings alternate dipping, 'biomimetic' precipitation [15] and even electrolysis [16]. All of these methods can be undertaken in almost ambient conditions. Although a number of workers have investigated the influence of processing on the crystallinity and purity of calcium phosphate salts [17, 18, 19], to date there has been relatively little work on the effect that these factors could have on cell attachment to the coating surface.

In this study, initial cell attachment and proliferation occurred more rapidly on Group A than on the Group B prosthesis. Systematic investigation of parameters known to influence cell attachment, such as topography and crystallinity, revealed that Group B had a more heterogeneous surface topography compared with Group A whilst the coating on Group A was of lower crystallinity. This suggests that purity and nanostructure of HA coated implant is the dominant factor over the surface topography for initial cell attachment. The mechanism of enhanced initial cell attachment and proliferation on the surface of the Group A prosthesis could be as a result of two or more complimentary factors both related to the specific surface area exhibited by the HA coating. It is well established that cells attach to proteins adsorbed onto the surface of materials [20]. The higher specific surface area exhibited by the Group A coating would have resulted in an increase in the quantity of protein adsorbed onto the surface and therefore may have stimulated greater cell attachment. The higher specific surface area of the material could also have resulted in the more rapid dissolution of the calcium phosphate coating on immersion in culture medium [14]. This dissolution would have resulted in an increase in the local concentration of calcium, a factor that is known to mediate the attachment of osteoblast-like cells to surfaces. This mechanism has also been shown to expedite the attachment of a range of cells to materials such as bioglass [21] and silicon substituted hydroxyapatite monoliths [22].

While a number of researchers have reported the formation of nanocrystalline coatings using processes at room temperature [13, 14, 15], relatively few have sought to tailor crystallinity to enhance cell attachment using a high temperature plasma. It is well established that introducing more energy into the system results in amorphisation of the calcium phosphate droplets [23], but this has previously been treated as an unwanted phenomenon, and most studies have sought ways to avoid it occurring as opposed to use this method to control cell attachment of the ceramic

surface. We have demonstrated that it is possible to adjust crystallinity in a monotonic manner with increasing anodic potential, without jeopardising the purity of the final coating and compromising biological activity.

5. Conclusion

Here we have shown that nanoscale crystallinity of HA based coatings is the dominant factor over the macroscale topography for initial cell adhesion and cell growth. We have also demonstrated that it is possible to adjust coating crystallinity by making small changes to processing, without compromising coating purity. It is possible that the findings of this study will be of utility in designing novel coated calcium phosphate surfaces that more rapidly bond to bone following implantation.

References

[1] Ohgushi H, Okumura M, Yoshikawa T, Inoue K, Senpuku N, Tamai S, Shors EC. Bone formation process in porous calcium carbonate and hydroxyapatite. J Biomed Mater Res. 1992;26:885-895.

[2] Hannouche D, Petite H, Sedel L. Current trends in the enhancement of fracture healing J Bone Joint Surg Br. 2001;83:157-164.

[3] Bauer TW, Muschler GF. Bone graft materials. An overview of the basic science. Clin Orthop Relat Res. 2000;371:10-27.

[4] Kroon PO, Freeman MAR. Hydroxyapatite coating of hip prostheses: effect on migration into the femur J Bone Joint Surg Br. 1992;74:518-522.

[5] Desmet T, Morent R, De Geyter N, Leys C, Schacht E, Dubruel P. Nonthermal Plasma Technology as a Versatile Strategy for Polymeric Biomaterials Surface Modification: A Review Biomacromolecules. 2009;10:2351-2378.

[6] Yang Y, Kim K-H, Ong JL. A review on calcium phosphate coatings produced using a sputtering process—an alternative to plasma spraying Biomaterials. 2005;26:327-337.

[7] Pálka V, Poštrková E, Koerten HK. Some characteristics of hydroxylapatite powder particles after plasma spraying Biomaterials. 1998;19:1763-1772

[8] Yang C-W, Lee T-M, Lui T-S, Chang E. A comparison of the microstructural feature and bonding strength of plasma-sprayed hydroxyapatite coatings with hydrothermal and vacuum post-heat treatment Mater Trans. 2005;46:709-715.

[9] Wang BC, Chang E, Lee TM, Yang CY. Changes in phases and crystallinity of plasma-sprayed hydroxyapatite coatings under heat treatment: A quantitative study. J Biomed Mater Res. 1995;29:1483–1492.

[10] Gross KA, Berndt CC. Thermal processing of hydroxyapatite for coating production J Biomed Mater Res.1998;39:580–587.

[11] Zhong JP, Greenspan DC, Feng JW. A microstructural examination of apatite induced by Bioglass® in vitro J Mater Sci: Mater Med. 2002;13:321-326.

[12] Sato M, Asiani A, Sambito MA, Kalkhoran N.M, Slamovich EB, Webster TJ. Nanocrystalline hydroxyapatite/titania coatings on titanium improves osteoblast adhesion. J Biomed Mater Res. 2008;84A:265-272.

[13] Balasundarm G, Sato M, Webster TJ. Using hydroxyapatite nanoparticles decreased crystallinity to promote osteoblast adhesion similar to functionalising with RGD. Biomaterials 2006;27:2798-2805.

[14] Sum L, Berndt CC, Khor KA, Cheang HN, Gross KA. Surface characteristics and dissolution behavior of plasma-sprayed hydroxyapatite coating. J Biomed Mater Res A. 2002;62:228-236.

[15] Habibovic P, Barrere F, Van Bitterswijk CA, de Groot K, Layrolle P. Direct formation of nanophase hydroxyapatite on cathodically polarised electrodes. J Am Ceram Soc. 2002;85:517-522.

[16] Shirkhanzadeh M. Biomimetic hydroxyapatite coating on metal implants. J Mater Sci Mater Med. 1998;9:67-72.

[17] Salimi MN, Bridson RH, Grover LM, Leeke GA. Effect of processing conditions on the formation of hydroxyapatite nanoparticles. Powder Technol. 2011;218:109-118.

[18] Murray MGS, Wang J, Ponton CB, Marquis PM. An improvement in processing of hydroxyapatite ceramics. J Mat Sci. 1995;30:3061-3074.

[19] Bose S, Saha SK. Synthesis and characterization of hydroxyapatite nanopowders by emulsion technique. Chem Mater. 2003;15:4464-4469.

[20] Howlett CR, Evans MDM, Walsh WR, Johnson G, Steele JG. Mechanisms of initial attachment of cells derived from human bone to commonly used prosthetic materials during cell culture Biomaterials, 1994;15:213-222.

[21] Cao W, Hench LL. Bioactive materials Ceram Int. 1996;22:493-507.

[22] Botelho CM, Brooks RA, Best SM, Lopes MA, Santos JD, Rushton N, Bonfield W. Human osteoblast response to silicon substituted hydroxyapatite. J Biomed Mater Res A. 2006;79A:723-730.

[23] Guipont V, Espanol M, Borit F, Llorca-Isern N, Jeandin M, Khor KA, Cheang P. High-pressure plasma spraying of hydroxyapatite powders Mat Sci and Eng A 2002;325:9-18.

Figure Captions

Figure 1. A population of cells attached to coated surfaces and tissue culture plastic and stained using Calcein AM.

Figure 2. Scanning electron micrographs of the surface of the calcium phosphate coatings on group A and B prostheses.

Figure 3. a.) White light interferometry images showing the surface topography of the calcium phosphate coatings on Group A and B prostheses and b.) the mean S_a values of each sample group.

Figure 4. X-ray diffraction patterns of coatings removed from the coated metallic prostheses. The coating removed from Group A samples was of lower crystallinity than that removed from Group B. Miller indices of the major diffraction peaks of HA are also presented.

Figure 5. A typical diffraction pattern indicating the presence of no crystalline impurity phases when prepared with varying anodic current.

.

Figure 6. The reduction in crystallinity of the coating applied to group B with varying anodic current.

Table Captions

Table 1. Crystallite size and fraction of crystalline phase of the three implant coatings estimated from the XRD data using equations 1 and 2, respectively. [a]Peak too weak to be fully identified from the background.

Table 2. Elemental composition of the surface coating determined using XRF.

Figure 1

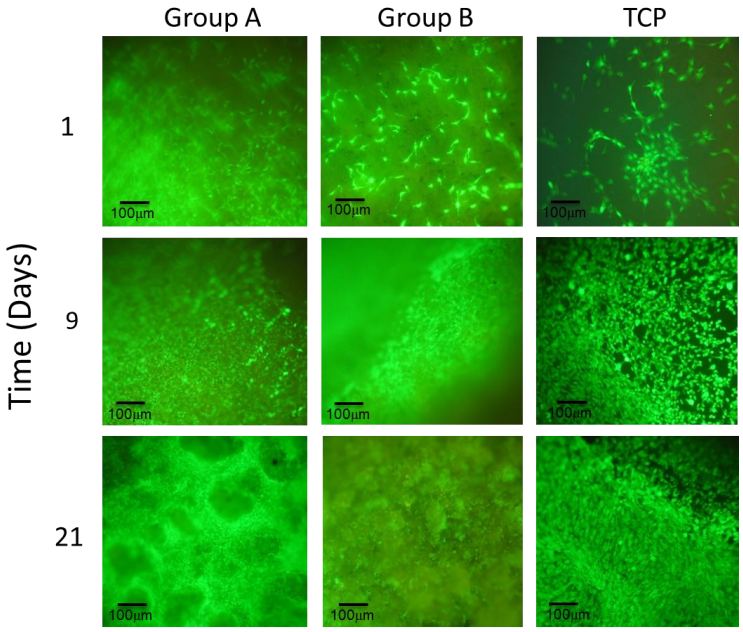

Figure 2

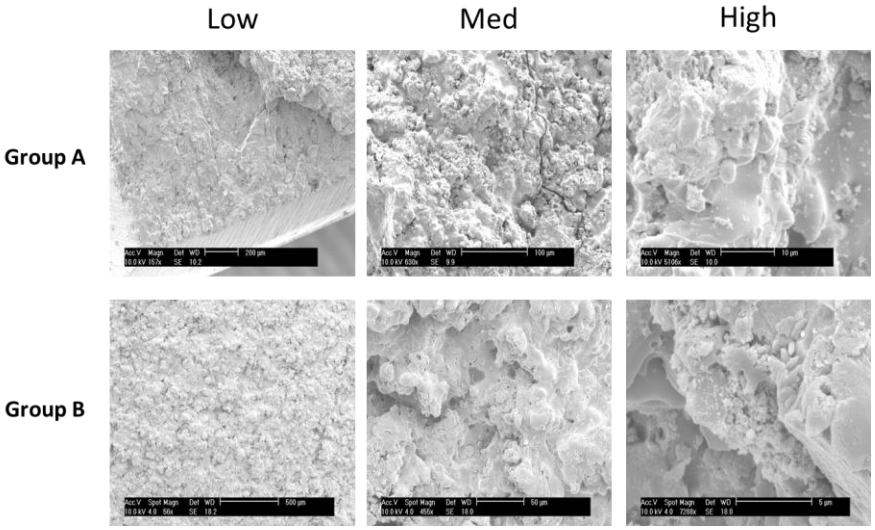

Figure 3

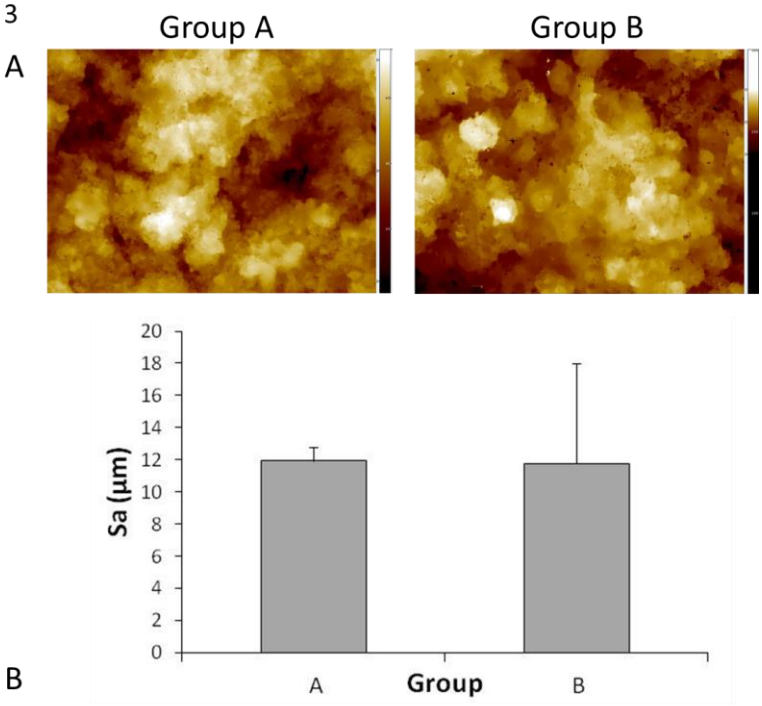

Figure 4

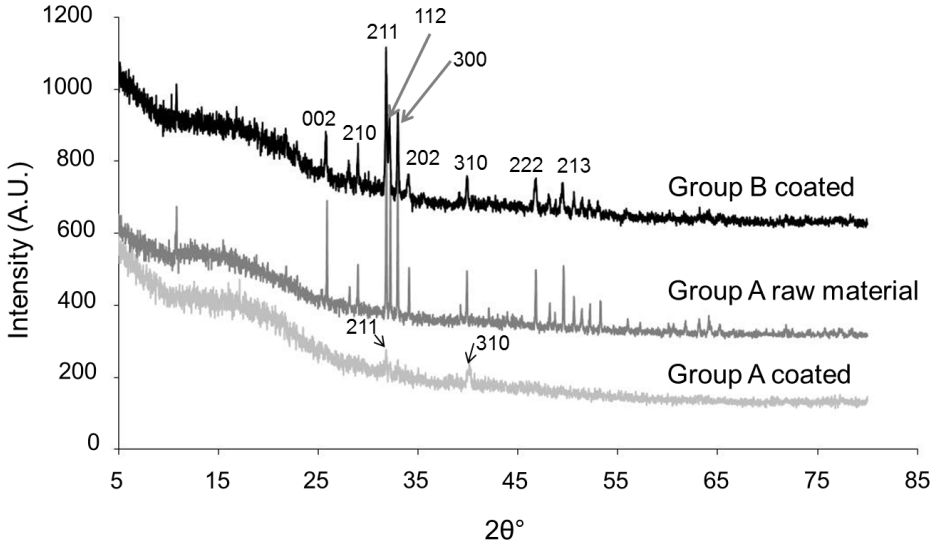

Figure 5

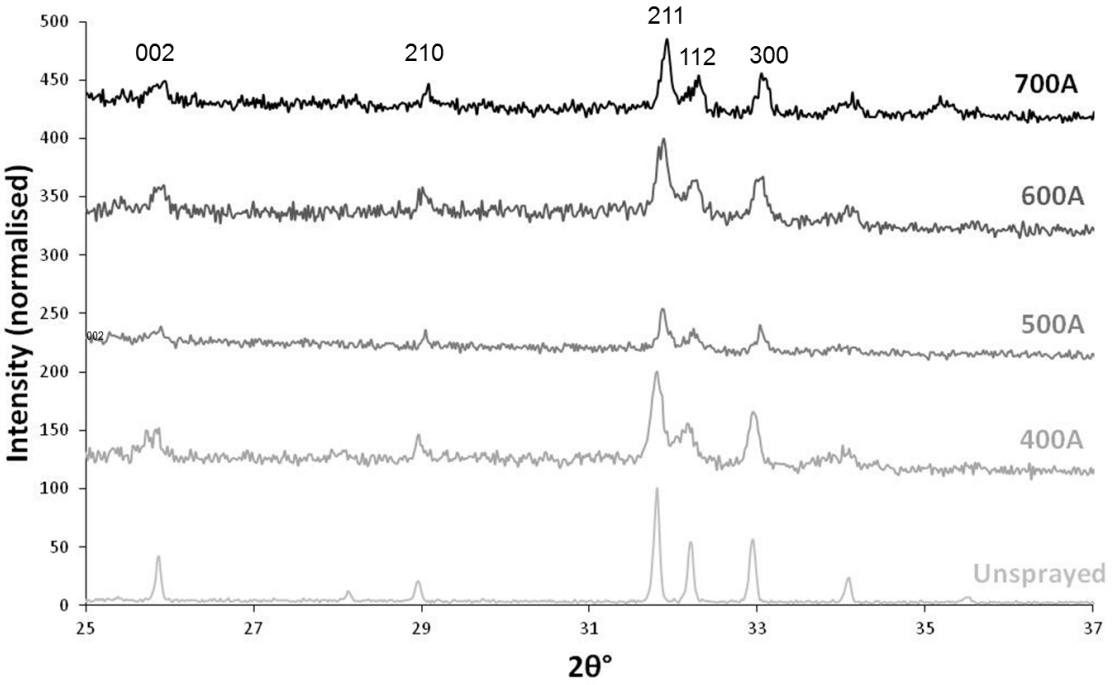

Figure 6

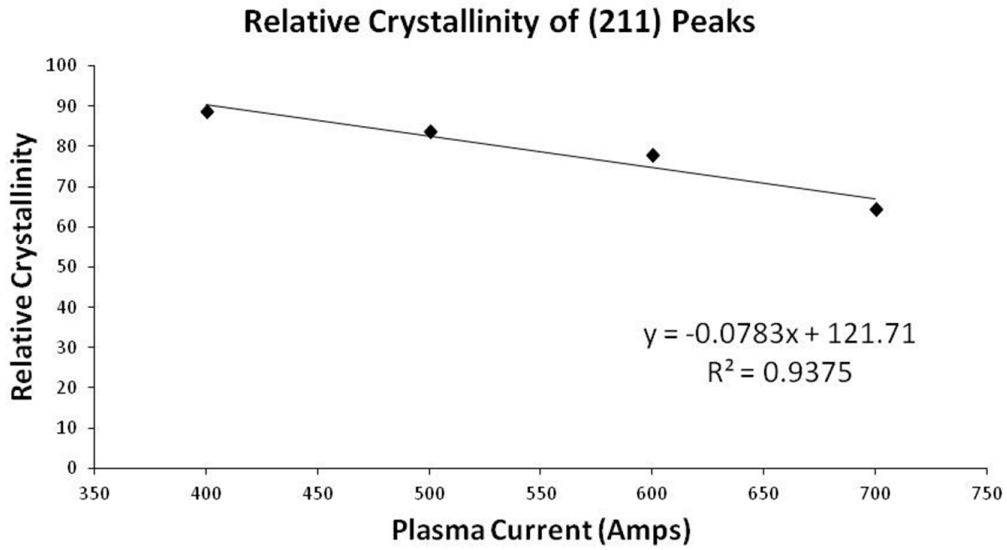

Table 1.

Sample	Crystallinity	Crystallite size (nm)	
		{002} plane (c-axis)	{300} plane (a-axis)
Group A - raw material	0.35	149.03	96.05
Group A	0.12	-[a]	25.28
Group B	0.26	55.95	48.04

Table 2.

Element	Mol %
Ca	76.8
P	21.6
Ti	0.6
Mg	0.5